Compositional convection caused by olivine crystallization in a synthetic basalt melt

JON K. SEEDHOUSE* AND COLIN H. DONALDSON

Department of Geology, St Andrews University, Fife KY16 9ST

Abstract

Compositional convection in magma chambers is thought to be an important process in the fractionation of liquid from crystals during the differentiation of magmas. It has been tested for in this study by undertaking isothermal crystal growth experiments in a silicate melt at atmospheric pressure in air. The melt used is a synthetic basalt in which iron is replaced by cobalt to minimise redox problems. Co-Mg olivine rims were overgrown on forsteritic olivine seeds cemented to the floor of a 2.4 cm deep alumina crucible. Following quenching and sectioning, glasses were examined optically for colour variations and by EPMA for compositional variations. It had been expected that the colour intensity of the blue glass would diminish in the Co-depleted zone that develops around crystal overgrowths, whereas in fact little difference is normally found, except for a slight fading of colour in glass above the apex of a seed in a few experiments. By contrast EPMA revealed zones up to 50 μm wide around seeds that are depleted in Co and Mg by up to 25 % at the crystal-glass interface and in patches above some crystals. Contour maps of X-ray count-rate data obtained in grids of analytical points show Co- and Mg-depleted glass around the overgrowths and in patches above the highest point of each seed, demonstrating that convection in the melt does occur during growth of individual crystals. As the experiments were carried out in a stable temperature gradient and the crystal seeds had no contact with the melt meniscus, thermal and surface-tensional convection are both eliminated, and the convection is inferred to be caused by a density difference resulting from compositional variation across the chemical boundary layer around a growing crystal. The density difference between the inside and outside of a boundary layer is calculated to be approximately −1%.

KEYWORDS: magma chambers, convection, olivine, basalt melt.

Introduction

TEMPERATURE differences in magma bodies have long been suggested as a cause of crystal–liquid fractionation (e.g. Wager *et al.* 1960). More recently, density variations due to compositional differences in melts have been proposed as an important mechanism bringing about transfer of matter in magma bodies by 'compositional convection' (e.g. Sparks *et al.*, 1984; Tait *et al.*, 1984; Martin *et al.*, 1987; Tait and Jaupart, 1992). Understanding of this process has developed through the use of experiments in which tanks of saturated, aqueous solutions are cooled and crystallized in an attempt to mimic magmatic solidification conditions (see reviews by Sparks *et al.*, 1984; Turner and Campbell, 1986).

In aqueous salt-solution experiments, differentiation into compositionally contrasting liquids has been brought about by convective removal of light residual liquids from growing crystals. The compositional differences that may drive convection can arise whenever a crystal grows or dissolves because the crystal and solution differ in composition. Thus the solution at the crystal–liquid interface becomes enriched in some constituents and depleted in others, creating a compositional boundary layer. In magmas, enrichment in iron in melt surrounding a growing plagioclase crystal would increase its density causing downward flow of melt from around the crystal (Fig. 1*a*). In contrast iron depletion in melt about growing mafic minerals would create a

*Current address; British Gas Research and Technology, Gas Research Centre, Ashby Road, Loughborough, LE11 3QU.

Mineralogical Magazine, February 1996, Vol. 60, pp. 115–130

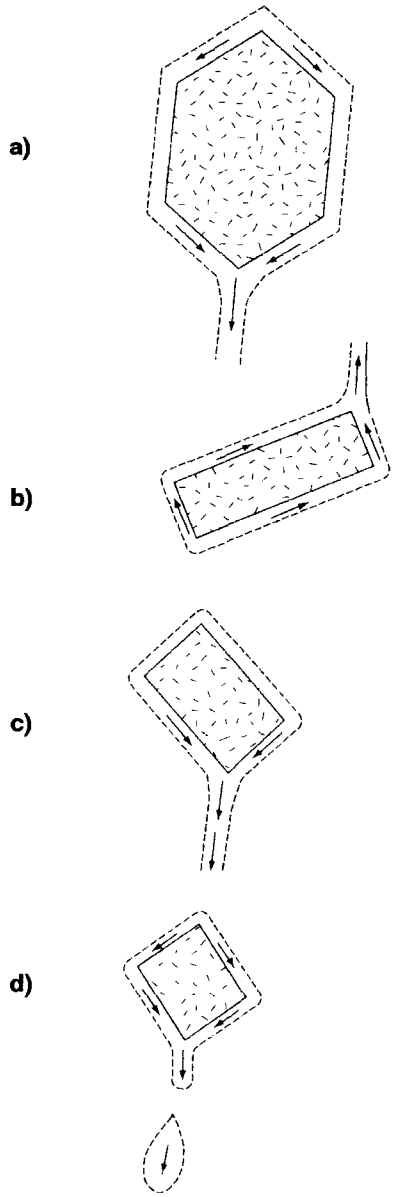

FIG. 1. Formation and convection of compositional boundary layers around growing or dissolving crystals. (*a*) Production of a higher density boundary layer by dissolution of mafic minerals or by growth of felsic minerals. (*b*) Production of a lower density boundary layer by dissolution of felsic minerals or by growth of mafic minerals. (*c*) Rapid production of boundary layers may result in the boundary layer melt leaving the crystal as a continuous plume/stream of melt, while (d) slow production may result in the material leaving the crystal as discrete blobs of melt.

'boundary layer' with a tendency to flow upwards because it is less dense than the host melt (Fig. 1*b*).

Such compositional boundary layers have been observed in quenched glasses surrounding phenocrysts in chilled basalts (Donaldson, 1975). They have also been detected in glass around partially dissolved crystals in various silicate systems by Kuo and Kirkpatrick (1985*a*,*b*), Brearley and Scarfe (1986), and Zhang *et al.* (1989) and their convective behaviour has been studied by Donaldson and Hamilton (1987) and Donaldson (1993).

The experiments described in this paper follow on from these dissolution experiments, and investigate the role that compositional convection driven by crystallization may play in magma systems. Whereas boundary layer formation and convection have been observed in crystallising aqueous salt solution experiments, crystallization experiments using silicate melts have not previously been reported. This study examines the production and convection of boundary layers around growing olivine crystals in a basaltic melt. This was done by undertaking a series of crystal-growth, quenching experiments with a synthetic basaltic melt under supercooled conditions (Seedhouse, 1994). The results show clearly that compositional convection has occurred, indicate that the magnitude of the density difference is capable of inducing convection, and also indicate the manner in which flow occurs.

Experimental procudure

To avoid problems with iron oxidation, and the associated compositional change of melts at high temperatures, an olivine-normative basaltic system was chosen that would not oxidise in an uncontrolled air atmosphere. This is a system in which iron is replaced by cobalt which is not subject to oxidation in air (Coons *et al.*, 1976; Coons and Holloway, 1979). This system was originally proposed as an analogue for natural basalts in experimental petrology because the amount of cobalt lost to noble metal containers is negligible compared with iron.

Coons *et al.*, (1976) report that equimolar replacement of Fe by Co produces a melt whose phase relations over a wide range of oxygen fugacities match those of the Fe-bearing system, except for a systematic elevation of temperatures by about 50°C.

The synthetic basaltic melt (liquidus 1265°C) used is modelled on that used by Coons *et al.* (1976), namely the 1921 Kilauea basalt (analyses A and B in Table 1). It was produced by combining and fusing oxides, carbonates and bicarbonates of the component elements. After fusing (at 1320°C for 2 hours per batch) and powdering the mixture twice, chips of

TABLE 1. Representative glass and mineral analyses from experimental charges. A = 1921 Kilauea basalt (Hill, 1969). B = cobalt basalt. C = olivine overgrowth. D = glass directly above crystal apex. E = boundary layer glass. F = melt at crucible wall. G = cobalt spinel. H = cobalt spinel

Weight%	A	B	C	D	E	F	G	H
SiO_2	49.4	48	36.2	49.5	50.6	48.5	0.1	0.4
TiO_2	2.78	3.4	0.1	3.4	3.8	2.4	0	0.3
Al_2O_3	13	12.6	0	15.7	15.3	21.1	65.6	45.5
FeOtot	12.3							
CoO		11.9	29.7	10.4	8.6	8	8.6	27.4
MgO	8.1	8.5	32.4	7.8	5.9	3.9	22.9	21.2
CaO	11.3	12.9	0.4	12.3	13	14.3	0	0.1
Na_2O	2.15	0.6	0.1	0.2	0.3	0.4	0	0
K_2O	0.52	0.3	0	0.2	0.2	0.2	0	0
Total	99.55	98.2	99	97.6	97.6	98.6	97.3	95.1

glass were analysed by EPMA and were found to be homogeneous within analytical error. Na_2O and K_2O values in the analogue are lower than those in the Kilauea basalt due to loss on fusion of the powdered mixture.

The Co-basalt glass is a brilliant royal blue colour due to the occurence of Co^{2+} in tetrahedral coordination (Coons *et al.*, 1976). Mafic minerals that crystallize from the melt are also vividly coloured in thin section, olivine is pink and pyroxene yellow. These colour differences in the crystals arise from differences in the shapes of the octahedra of oxygen atoms surrounding Co^{2+} ions in each phase (Coons *et al.*, 1976).

The natural (Fe-Mg) olivine crystals used are of Fo_{90} composition and *ca.* 3–4 mm in length. They were made elongate by grinding prism and pyramid-type 'faces' onto each crystal.

Experiments were carried out in cylindrical alumina crucibles (18 mm internal diameter and 24 mm height) in which olivine seeds were cemented to the base with alumina cement. Previous experimental work (Donaldson, 1993) indicated that this method should be restricted to short-duration runs because basaltic melt dissolves the cement enabling the crystal seed to escape. At the lower temperatures used in the present study (1230–1250°C versus >1300°C used by Donaldson), and using an iron-free melt, the rate of alumina dissolution was so greatly reduced that the problem of escaping crystals rarely arose. This decreased rate of alumina dissolution also allows us to dismiss the possibility of such a reaction producing an Al_2O_3 rich melt which could display low density convective behaviour.

Olivine crystals were cemented to crucible floors with long axes approximately vertical. Unlike the boundary layer adjacent to a horizontal crystal face, low density boundary layer melt produced on an inclined surface can never be stable (Martin *et al.*, 1987). The chosen shape and alignment of the olivine seeds therefore encourages rapid onset of flow of boundary layer melt and maximises the chance of detecting compositional-driven convection.

A crucible is loaded onto the plinth of the furnace hearth and then raised into the furnace. To quench the charges, the bottom of the furnace is lowered and the charge lifted onto a silica mat at room temperature. As the furnace hearth lowers, the meniscus changes from yellow-red to black in appearance; the quench rate over this period is estimated as 60°C s^{-1}. As the furnace has a hydraulically-operated elevator hearth, its smooth motion prevents jerking as the charge is lowered from the furnace which inhibits any forced convection occurring during quenching.

To ensure that any inferred convection is due to compositional differences in the melt, all other possible causes of convection must be suppressed in the experimental charges. Convection driven by temperature variation is eliminated by carrying out experiments in a temperature gradient in which the top of the crucible is 4°C hotter than the bottom, ensuring a stable density gradient due to the highest density melt being on the bottom. [Soret diffusion over such a small temperature gradient would be negligible in the short run durations used in most of these experiments and so is not considered to be a possible indirect thermal cause of compositional convection.] Possible convection due to variations in surface tension associated with the melt meniscus (Donaldson, 1993) is eliminated here by ensuring that the crystal seed never comes into contact with the meniscus.

Analysis of experimental charges

Co^{2+} concentration in the synthetic basalt is reflected by the intensity of the colour of the glass. It was hoped that Co-depletion in the boundary layer adjacent to a crystal overgrowth would be sufficient to make the layer visible as a paler blue colour in thin section. However a few experiments were sufficient to establish that the combination of a small compositional difference in glass at the crystal-glass interface and the narrow width of the boundary layer make it hard to detect optically. Some areas of paler blue glass well beyond a crystal were detected in sections that were inadvertently polished thinner than usual (down to 20 μm) and these areas were targeted for electron probe analysis.

A JEOL JCXA 733 Superprobe microanalyser was used for glass analysis. Back-scattered electron imagery (BSEI) and wavelength-dispersive spectrometry were used to examine compositional variations in the quenched runs. Operating conditions for analysis were 15kV and 20nA throughout, using pure metals, oxides and minerals as reference standards and a 1μm diameter electron beam. Apparent concentrations were corrected using conventional ZAF correction procedures.

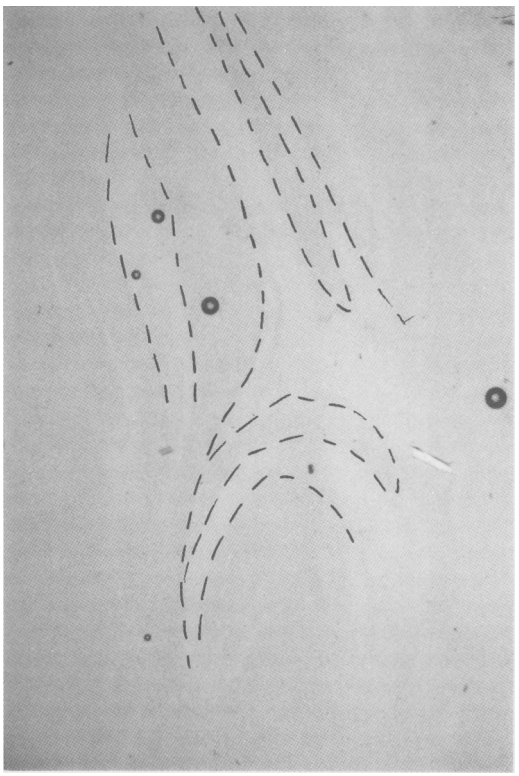

FIG. 2. Plane-polarized light photomicrograph of glass above the crystal apex in experiment B (1230°C for 72 hours). The photograph shows the streaky appearance of the glass with swirls emphasised in ink. Paler areas represent CoO-depleted glass derived from the compositional boundary layer at the crystal-glass interface. Field of view is 3 mm wide.

Initially full quantitative analysis was carried out on some runs to determine both glass and mineral compositions (see Table 1 for representative analyses). Analyses (compare analyses B and E in Table 1) indicated that the composition of glass at the crystal-glass interface differs from that far from the crystal and that the compositional boundary layer to a crystal is very narrow (<50 μm). Subsequently a different approach to analysis was adopted which involved closely-spaced points being analysed for just Co and Mg, without ZAF corrections being applied. Instead, the X-ray count rates at individual points were compared with the rates for known Co and Mg concentrations to obtain wt. % concentrations. Stage movement between points can be set at 1, 2, 5 or 10 μm; by this means the width of boundary layers can be determined to a few μm.

The X-ray count-rate data are displayed here graphically and as contoured maps. The contoured maps were produced using the programme called "UNIRAS, UNIMAP 2000" (source of software - AVS/UNIRAS Limited). This allows data from several analytical profiles to be brought together on a single map, so producing contoured maps of Co and Mg concentrations around apices of crystal seeds and at the meniscus of experimental charges.

Results

Run products

Run products consist of olivine seeds rimmed with a pink Co-olivine overgrowth, pink olivine crystallites in the lower reaches of the charges set in blue glass, and a thin dark band of minute euhedral spinel crystals lining the crucible walls and the alumina cement that supports the olivine seed. In only a minority of products is glass above the olivine overgrowths locally paler in colour (Fig. 2). At 1230°C crystallites of pink olivine only appear below the level of the crystal apex and do not hamper the search for fractionated glass above the olivine seed. In lower temperature runs, however, crystallites nucleate throughout the glass thus interfering with EPMA of glass above the apex.

Overgrowth morphology is a function of degree of supercooling, while overgrowth width is controlled by both degree of supercooling and time. At supercoolings >50°C, overgrowths have a complex

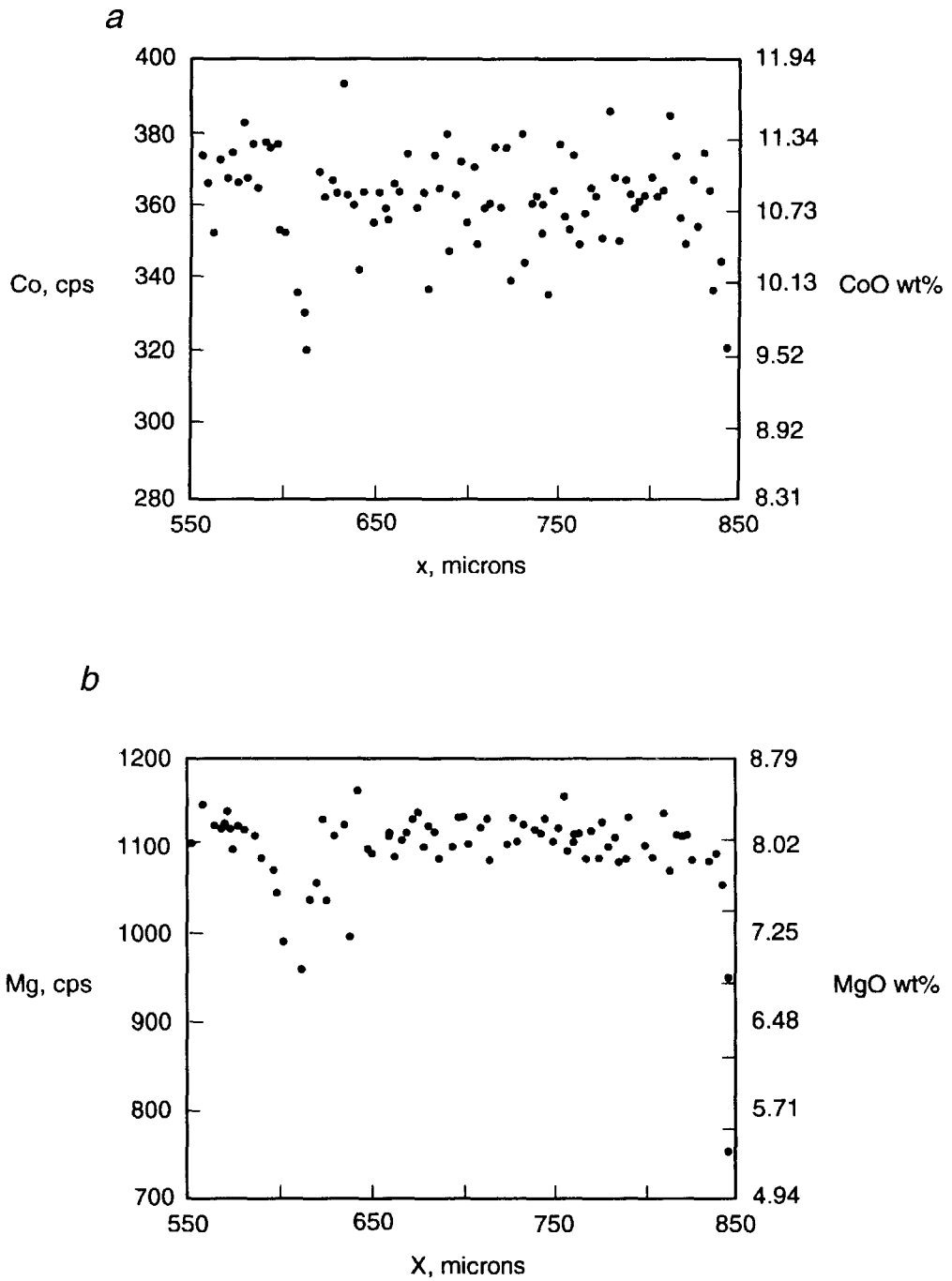

FIG. 3. CoO (*a*) and MgO (*b*) data from a horizontal profile running out for 300 m from the olivine-glass interface in experiment B. A 30 μm boundary layer of CoO and MgO-depleted glass is seen at the interface at the right hand side of the plot (× = 850 μm). The fall in both CoO and MgO concentrations at 600 μm occurs as the profile comes close to an olivine crystallite that has grown in the melt. This may be evidence for individual crystallites producing their own boundary layers.

porous, skeletal morphology and round edges and corners. With decreasing degree of supercooling the overgrowth morphology becomes more euhedral and less porous, and edges and corners are more angular. At small supercoolings the overgrowth has no holes. This morphological change with supercooling is consistent with the experimental results of Donaldson (1976). Morphology of the crystallites and that of the overgrowth are always similar implying that crystallites grew during the experiments rather than on quenching.

Approach to EPMA

Full analysis was carried out around the olivine overgrowth in experiment B (contrast analyses B and E in Table 1). The graphs in Fig. 3 show that an area of Co- and Mg-depleted glass is present adjacent to the crystal overgrowth; note that the interface between olivine and glass is at the right hand side of the profile. Both Co and Mg locally fall by up to 25% in a narrow (< 50 μm wide) zone, indicating that the pale glass (such as that identified above the crystal in Fig. 2) is also Co and Mg depleted, resulting from olivine crystallization.

Through the rest of the traverse in Fig. 3 a great deal of background 'noise' can be seen. This effect is smoothed out by the mapping technique by giving decreasing degrees of importance to neighbouring points as distance increases. The other major dip in Co concentration in this track occurs directly above an olivine crystallite in the glass (at 600 μm). The dip may be caused by release of Co-depleted boundary layer from that crystallite, or possibly by the Co-stripping effect of an olivine crystallite lying out of the plane of this section.

Description of three experiments

The data presented in this section are from three representative experimental runs (details in Table 2). Locations of EPMA traverses in each charge are presented in Figs. 4*a*–*c*. Shaded areas on these maps denote regions of detailed X-ray count rate analysis from which contoured maps were produced. A photograph of the run product is shown in Fig. 5. This is from experiment A but is representative of all experiments.

Experiment A, 1230°C for 24 hours. Figures 4a and 5 identify an area of glass in the thin section of this run product that shows slight colour variation. Directly above the crystal apex there are vertical streaks of pale glass. An analytical profile at the side of the overgrowth (Fig. 6) reveals a zone of just 15 μm width depleted in Co and Mg relative to the bulk glass, CoO is 5.3 wt% at the interface and 6.5 wt% beyond the depleted zone, with equivalent MgO values of 5.5 and 7.2 wt%. These values rise to 11 wt% and 8 wt% respectively further away (200 μm) from the crystal overgrowth. Quench crystal growth is unlikely to be the cause of this depletion as there are no dendritic projections on the overgrowth.

Preliminary traverses for Co and Mg identified a 5 × 4 mm area of glass above the seed suitable for

TABLE 2. Run conditions and products of experimental runs A, B, and C

Experiment	Run temp (°C)	Duration (hrs)	Notes	Number of X-ray analyses
A	1230	24	Pale blue glass visible above crystal apex and down sides of olivine seed. Pale glass not visible at meniscus. Olivine crystallites only present in lower reaches of charge. 50 micron olivine overgrowth around seed.	750 data points analysed on 5 lines of transect.
B	1230	72	Glass too thick to determine any colour variations above the crystal apex or at the meniscus. Olivine overgrowth approximately 100 microns thick.	400 data points on 4 lines of transect in glass directly above the crystal apex. 470 data points on 4 lines of transect in glass immediately beneath the meniscus.
C	1230	557	Thick pink olivine overgrowth. Up to 300 microns thick. Glass too thick to observe any colour variations.	530 data points on 5 analytical tracks in glass directly below the meniscus.

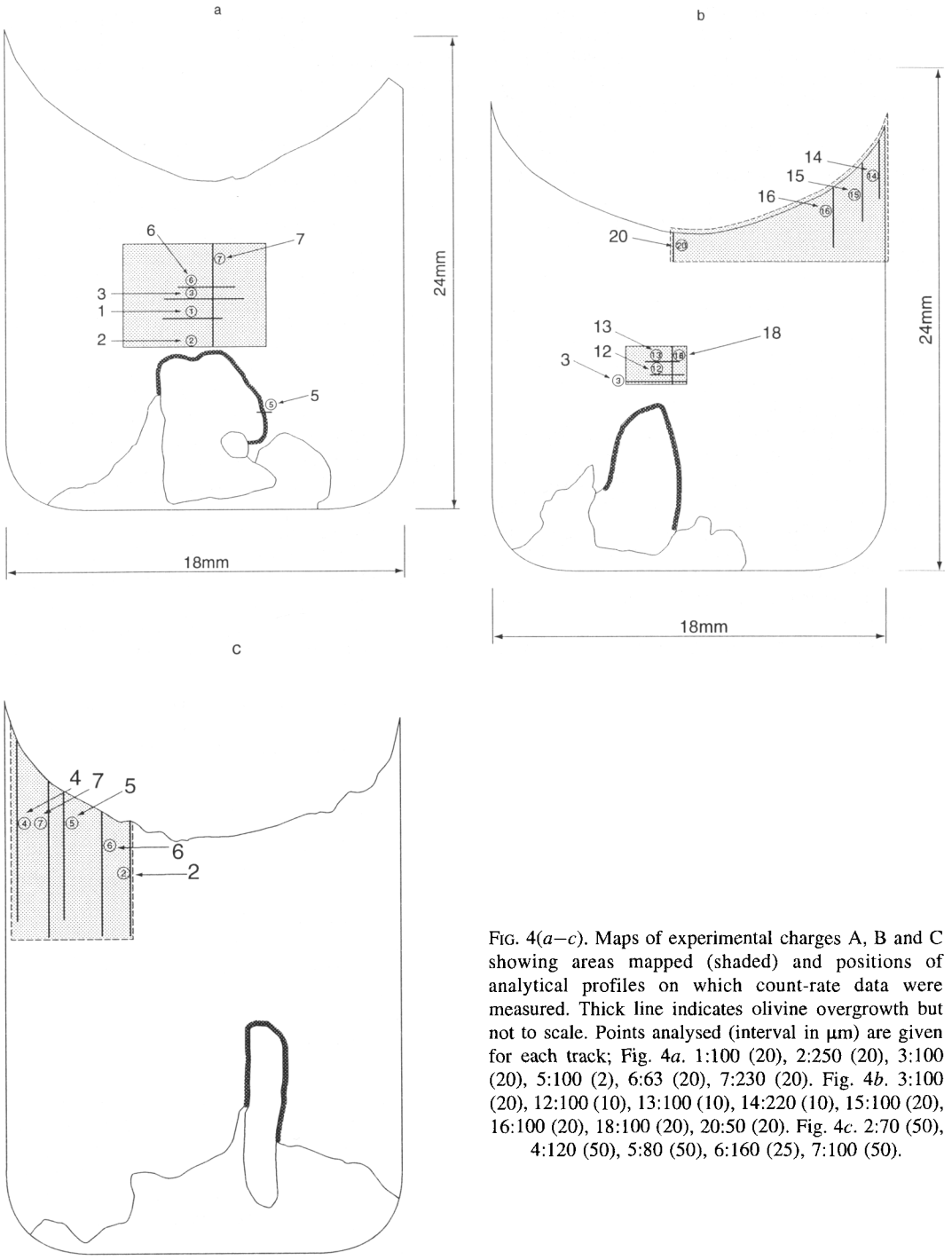

FIG. 4(*a*–*c*). Maps of experimental charges A, B and C showing areas mapped (shaded) and positions of analytical profiles on which count-rate data were measured. Thick line indicates olivine overgrowth but not to scale. Points analysed (interval in μm) are given for each track; Fig. 4*a*. 1:100 (20), 2:250 (20), 3:100 (20), 5:100 (2), 6:63 (20), 7:230 (20). Fig. 4*b*. 3:100 (20), 12:100 (10), 13:100 (10), 14:220 (10), 15:100 (20), 16:100 (20), 18:100 (20), 20:50 (20). Fig. 4*c*. 2:70 (50), 4:120 (50), 5:80 (50), 6:160 (25), 7:100 (50).

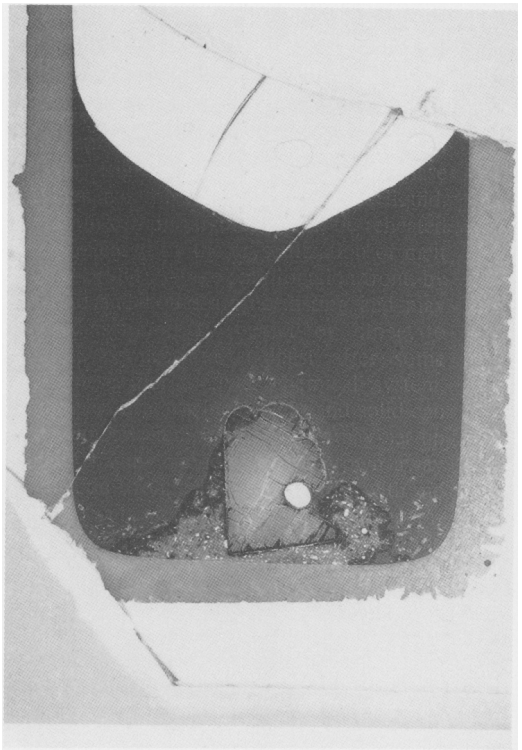

FIG. 5. Plane-polarised light photomicrograph of experimental charge A. Note the thin olivine overgrowth (pale grey) around the seed, and the slightly paler glass around and above the olivine seed. Width of crucible is 18 mm, total height of crucible is 24 mm. The appearance of this crucible is representative of all experimental charges.

compositional mapping (Fig. 4*a*). The map in Fig. 7 reveals a vertically-elongate region of Co-depleted glass above the crystal apex which is interpreted as a plume of melt that flowed from the boundary layer around the olivine seed. Contours give the plume a boudinaged form which may reflect an irregular three-dimensional structure, ie the plume may curve in and out of the plane of the section, or it could be caused by pulses of melt rather than a continuous stream leaving the crystal apex. Another point to note in Fig. 7 is the appearance of a second region of slightly Co-depleted glass on the left-hand side of the mapped area. This glass is above the top-left corner of the crystal seed and indicates that buoyant boundary layer melt detached not only from the highest point on the crystal; several plumes may have been active.

This experiment shows that a Co-depleted boundary layer is produced by olivine growth on crystal seeds, and that the melt from such a layer detaches from the upper reaches of the crystal and convects buoyantly. The following experiments provide information regarding whether or not such melt can remain discrete as it convects buoyantly to the meniscus.

Experiment B. 1230°C for 72 hours. (See Fig. 4*b*). Slightly paler glass is visible above the crystal apex in this longer duration experiment. Two areas were selected for compositional mapping (Fig. 4*b*), that above the apex as well as that directly beneath the meniscus, to check whether rising Co-Mg-depleted plumes had caused compositional differentiation in the charge.

The contour map observed from X-ray counts in the glass above the crystal apex (Fig. 8) again shows vertically elongated areas of Co depletion. As with experiment A, the indication is of release of boundary layer melt from the upper parts of the seed, and probably in pulses rather than as a continuous plume of melt. This map indicates that olivine growth was still occurring after 3 days.

If an Fe-bearing melt had been used, oxidation of the melt at the meniscus could have occurred, potentially inducing surface tension-driven convection. This does not happen in the Co-basalt and so any compositional variation that occurs at the meniscus must be produced by another mechanism. Fig. 9 is a map of Co concentration in glass directly beneath the meniscus in experiment B (cf. Fig 4*b*). Two regions of Co-depleted melt have been identified, neither of which is evident in optical examination. These areas are discrete and are at the lowest and highest parts of the meniscus. That at the lower part of the meniscus could be due to collection of plumes of buoyant boundary layer melt from the growth of the olivine. The Co-depleted glass at the top of the meniscus could have been produced by this melt rising along the meniscus to the highest point. Another explanation, however, is possible for the Co-depleted glass at the top of the meniscus. The walls of the alumina charge are lined with a rim of euhedral cobaltous spinel crystals (see analyses G and H in Table 1). Analysis of the glass adjacent to these crystals (compare analyses B and F in Table 1) indicates that it is Co depleted. Co-spinel crystallization on the crucible walls produces a side-wall zone of Co-depleted, and Al-enriched melt. The alumina enrichment is due to Co and Mg being taken out of the melt during hercynite crystallization while Al, dissolved from the crucible walls, goes into the melt. Being depleted in Co, this melt has a lower density than the bulk melt and should therefore be buoyant. Compositional convection of this melt could have been partially or wholly responsible for the Co-depleted glass at the highest part of the meniscus.

Experiment C. 1230°C for 557 hours. Figure 4*c* indicates the position of the glass targeted for

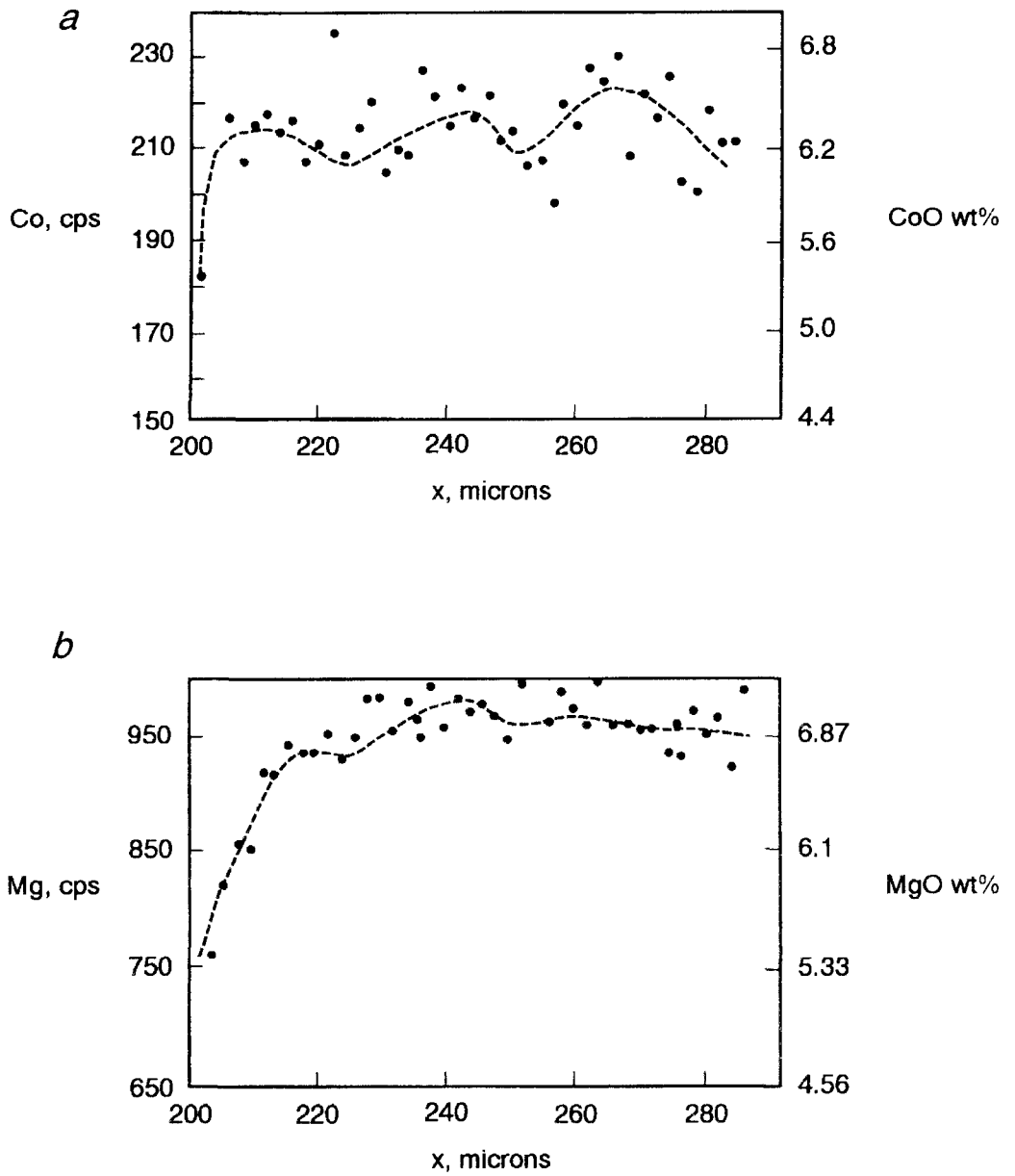

FIG. 6. Plots of distance from crystal-glass interface versus cobalt and magnesium concentrations in track 5 in experiment A. Note the thin zone of depletion (10 μm for CoO and 20 μm for MgO) at the left hand side, closest to the olivine overgrowth.

analysis in this experimental charge. A run of almost 3 weeks duration was undertaken to explore the extent of compositional-driven fractionation of melt.

Mapping immediately above the apex of the crystal revealed that no plume was present, suggesting that olivine growth had ceased in this long-duration experiment. Nonetheless, the map in Fig. 10 of the concentration of Mg in the glass beneath the meniscus in the uppermost reaches of the experimental charge shows that glass in this region is compositionally

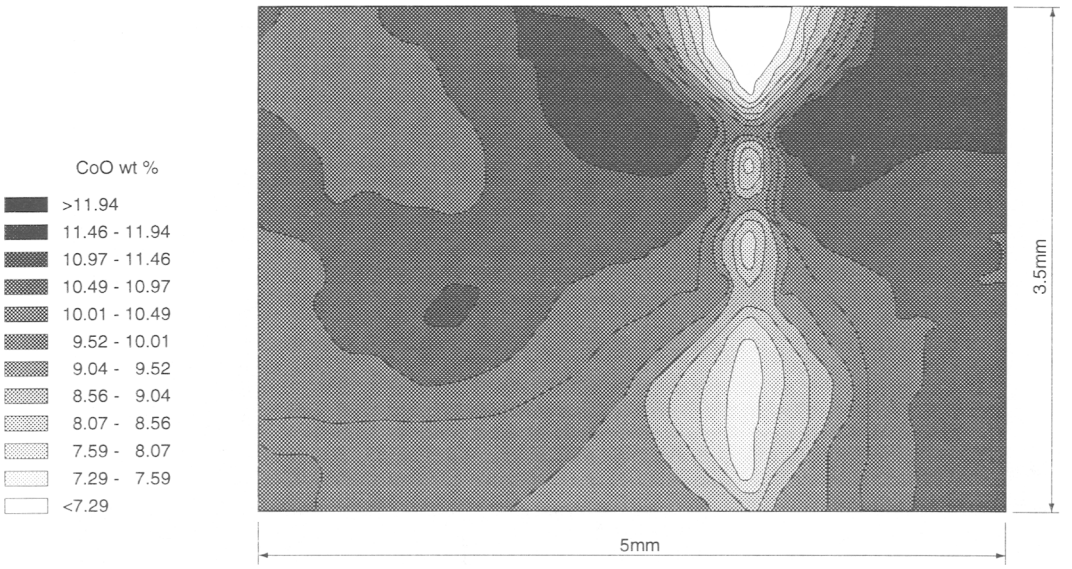

FIG. 7. Map of cobalt concentration in glass above the olivine seed in experiment A. The database for this map comprises 750 data points from five traverses. Note the boudinaged form of the CoO-depleted glass directly above the position of the crystal apex. This may be indicative of pulses of boundary layer melt convecting buoyantly from the crystal apex.

layered, with the most Mg-depleted melt occurring in the highest parts of the charge. The layer of depleted melt stretches right across the meniscus.

Mg-depleted glass can also be identified at the side of the crucible on the left of this map. Mg depletion in this patch of glass is probably the result of side-wall Co-spinel crystallization producing a zone of buoyant, side-wall boundary layer melt.

From the data in Fig. 10 it can be inferred that differentiation of melt, driven by compositional (and therefore density) differences, has occurred during this experiment. The compositional differences are the result of two independent crystal growth processes which both extract Co and Mg from the synthetic basaltic melt, growth of Co-Mg olivine on the crystal seed, and crystallization of Co-spinel on the crucible wall.

Discussion

Density and viscosity variations

Figure 11 shows calculated density and viscosity profiles for melts adjacent to olivine overgrowths in experiment B. These profiles show that melt density decreases and viscosity increases in the compositional boundary layer towards the olivine. Across this 50 μm zone, density decreases from 2.750 to 2.728 g/cc (1.7%) and viscosity increases from 180 to 310 poise, resulting in a thin layer of melt physically and chemically distinct from the melt around it.

Figure 12 displays horizontal profiles of melt density and viscosity variations derived from analyses of glass above the crystal apex in experiment B. These profiles show a density decrease and viscosity increase in the glass. Viscosity increases by 50% and density decreases by about 1% across these areas. These data indicate that only small density differences (<1%) are sufficient to cause convection that produces measurable compositional effects in a low viscosity, basaltic melt.

An estimate is possible of the maximum rate of ascent of a plume of paler blue, Co-depleted melt above the apex of an olivine seed. Taking the plume diameter as 4 mm and the densities of melt in the plume and beyond it as 2.746 and 2.752 g cm^{-3}, respectively (Table 3), and the viscosity of the melt through which the plume is moving as 240 poise, Stokes Law gives the terminal velocity as 3cm hr^{-1}. Clearly reasonably rapid ascent would be possible if the plume can rise far enough to accelerate to the terminal velocity.

Manner of release of boundary layer melt

Figures 1*c,d* outline the manner of release of boundary layers from growing or dissolving crystals. Release of melt may be as a continuous stream or as

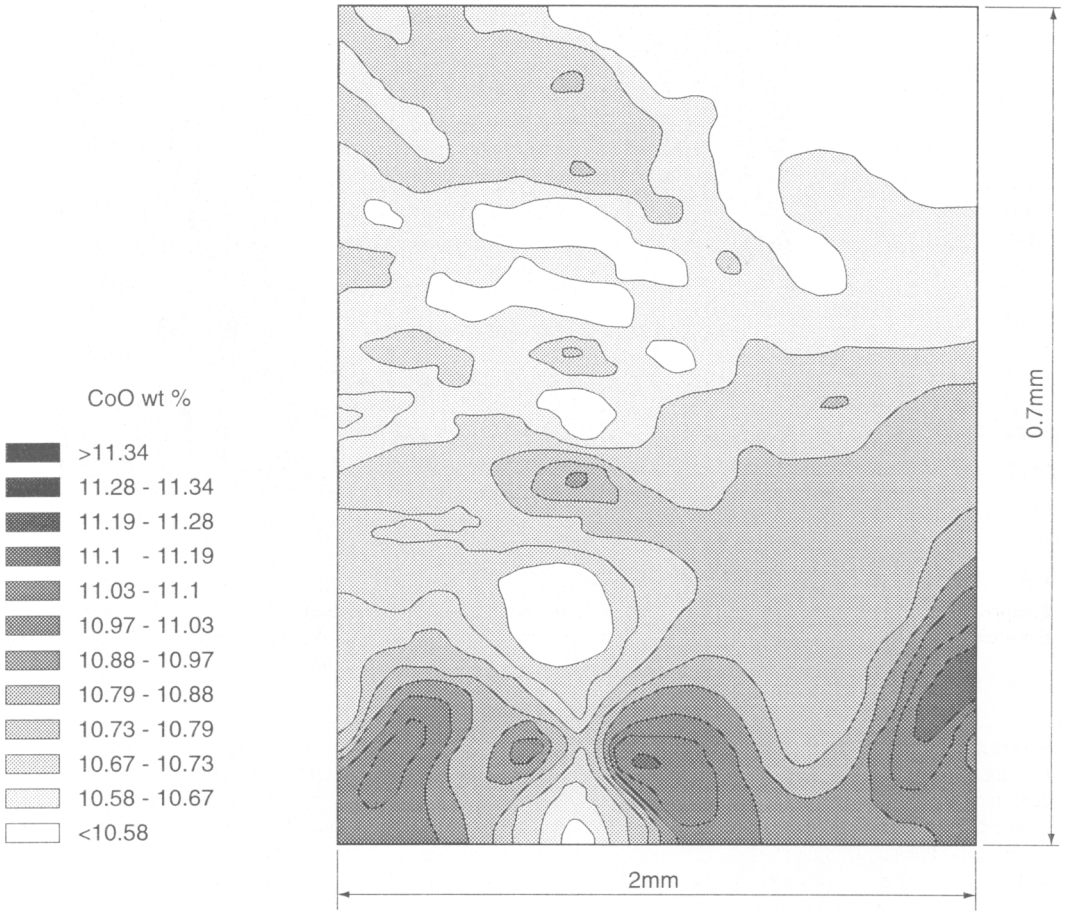

FIG. 8. Map of cobalt concentration in glass above the crystal seed in experiment B. Note the blobs of depleted melt directly above the crystal apex, indicating that boundary layer melt is being produced by olivine growth and is convecting buoyantly. The map contains data from 400 analytical points in an area of glass 2 mm × 0.7 mm positioned 1 mm above the crystal apex.

TABLE 3. Compositional Rayleigh number calculations for boundary layer development adjacent to a horizontal olivine surface in a synthetic basalt. The thickness at which the boundary layer becomes unstable at a given diffusion coefficient is shown along with the time taken for this thickness to be attained

Calculation	A	B
Density of interface melt (g/cm^3)	2.746	2.746
Density of original melt (g/cm^3)	2.752	2.752
Density Difference (kg/m^3)	6	6
Kinematic Viscosity (m^2/s)	74	74
Diffusion Coefficient (m^2/s)	10^{-9}	10^{-12}
Width of boundary layer (microns) required for $Ra_c = 1000$	10 790	1079
Time to develop the unstable width (hours)	116 000	1 160 000

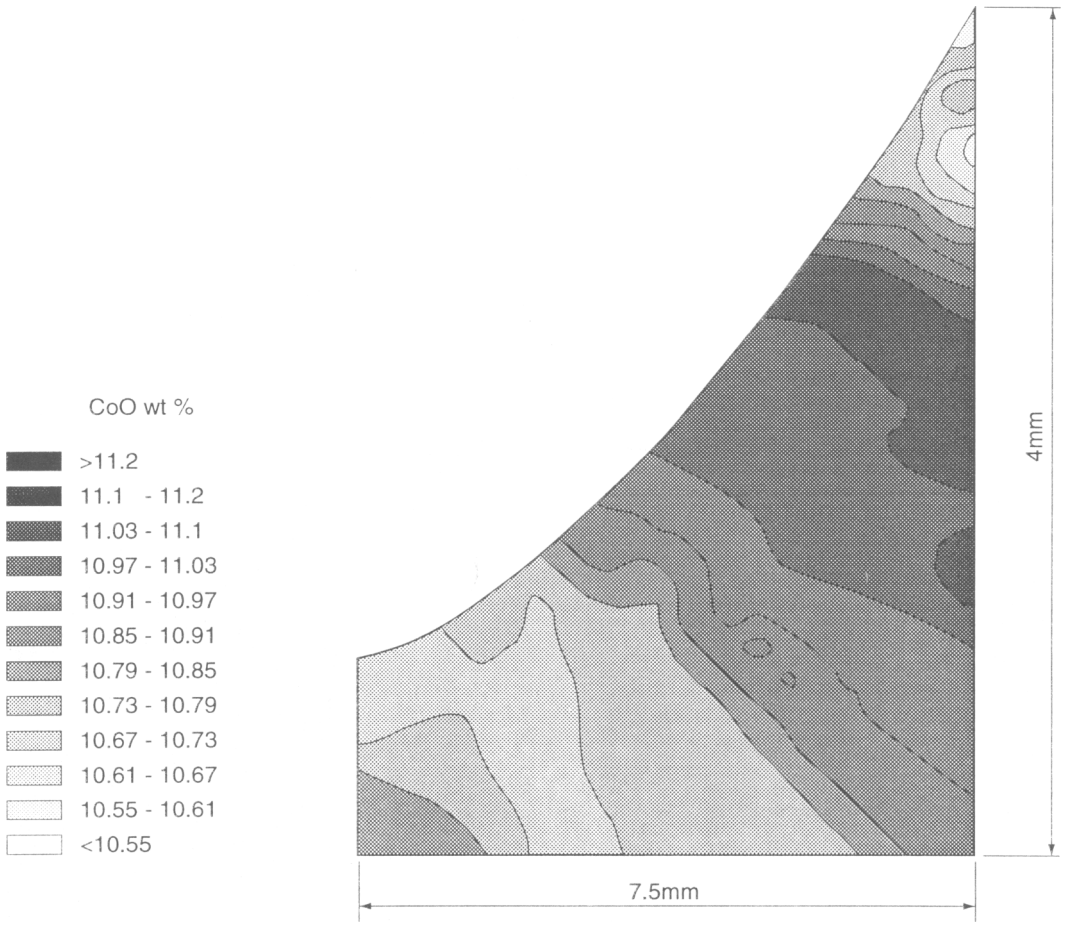

FIG. 9. Map of cobalt concentration (470 data points) directly beneath the meniscus in experiment B. Note the two regions of depletion; at the highest part of the meniscus and at the trough. CoO depletion at the upper corner could be the result of spinel crystallization on the crucible walls, while that at the lower part of the meniscus could only be formed by olivine crystallization on the seed.

punctuated packets. Fast crystal dissolution in relatively low viscosity melts favours continuous plume activity, while slow growth or dissolution in a viscous melt is more likely to produce periodic release of boundary layers from the top or bottom of the crystal (Donaldson, 1993). The evidence from the present crystallization experiments is not definitive on this issue. Compositional maps indicate that plumes are boudinaged in two-dimensional form but as previously commented they may be continuous in three dimensions. The only way of resolving this uncertainty would be to undertake the laborious task of multiply sectioning the crucible and building up several parallel maps to investigate the three-dimensional form of the depleted melt.

Petrological relevance

The products of experimental runs cannot be regarded as models for magma chambers, as experiments only study convective fractionation around individual crystals. However the results show, for the first time, that compositional convection caused by crystallization can take place in silicate melts. The experiments show that minute density variations in thin boundary layers can drive convection in basaltic melts.

In this study, elongate crystal seeds have been used and the boundary layer melt that they produce feeds upwards to a plume that drains boundary layer melt away from the crystal. Martin *et al.* (1987) described

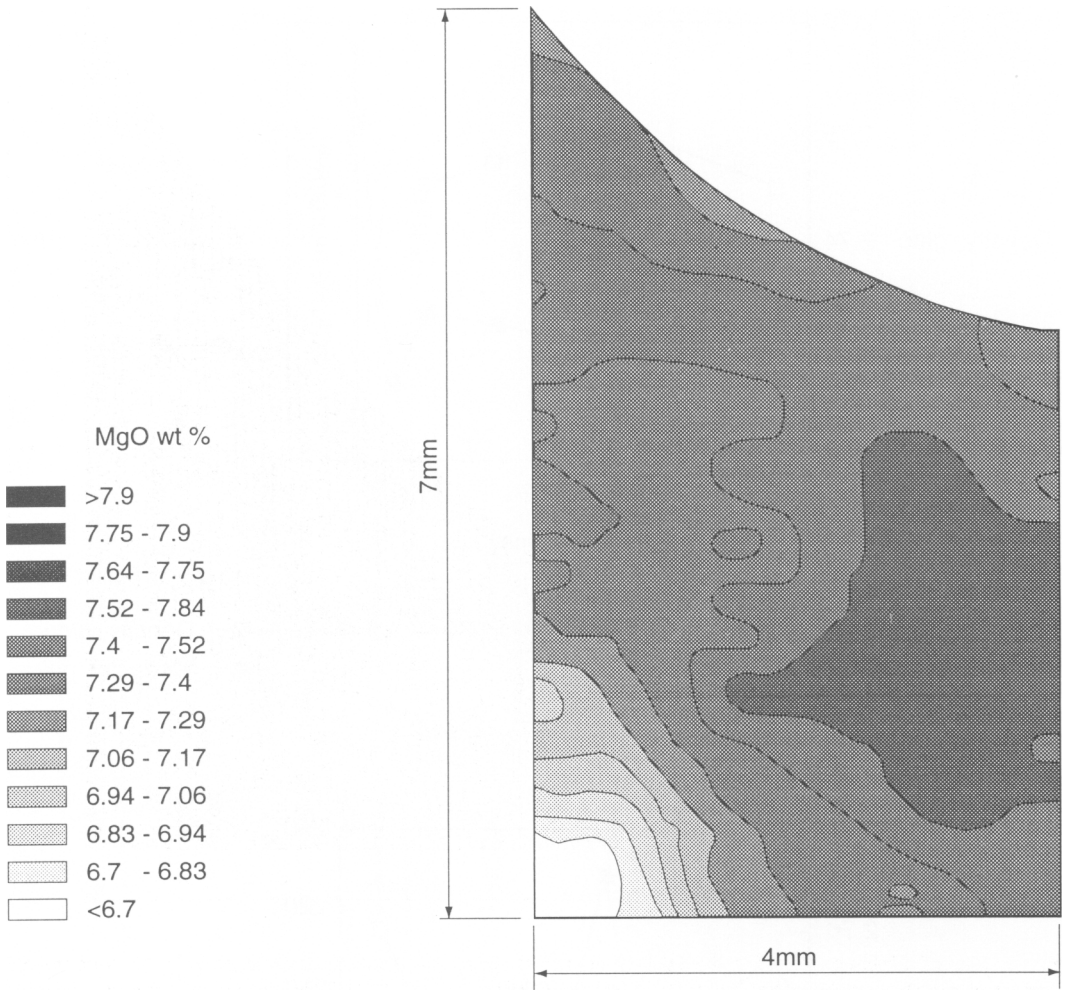

FIG. 10. Map of MgO concentration beneath the meniscus in experiment C. Note that depleted melt has ponded at the highest part of the charge, producing a compositionally-layered charge.

how a layer of equant, closely-spaced olivine crystals growing on the floor of a magma chamber might combine their individual boundary layers to produce a layer of Mg- and Fe-depleted melt, covering the crystals (their Fig. 7). This zone of melt could convect away by building up a thickness at which its compositional Rayleigh number exceeds 1000, or it could be swept away by convective currents in the magma chamber. The stability of a boundary layer on a horizontal surface is governed by the compositional Rayleigh number, Ra_c, where;

$$Ra_c = g\Delta\rho_c\, d^3/\nu D.$$

This value must exceed 1000 for boundary layer instability (Sparks *et al.*, 1984). In the equation g is the gravitational constant, $\Delta\rho_c$ is the compositional density difference across the film, d is the boundary layer thickness, ν is the kinematic viscosity, and D is the chemical diffusion coefficient. Values for ν and $\Delta\rho_c$ have been calculated from melt compositions. Values for D are in the range $10^{-9} - 10^{-12}$ m^2s^{-1} (Hofmann, 1980.) The computed densities and viscosities for experiment B have been used to calculate values for d from the Rayleigh equation and the times needed for a boundary layer to grow to these thicknesses (Table 3). The times taken for boundary layers to reach unstable thicknesses are calculated using the equation T (hours) $= d^2/D$ for the

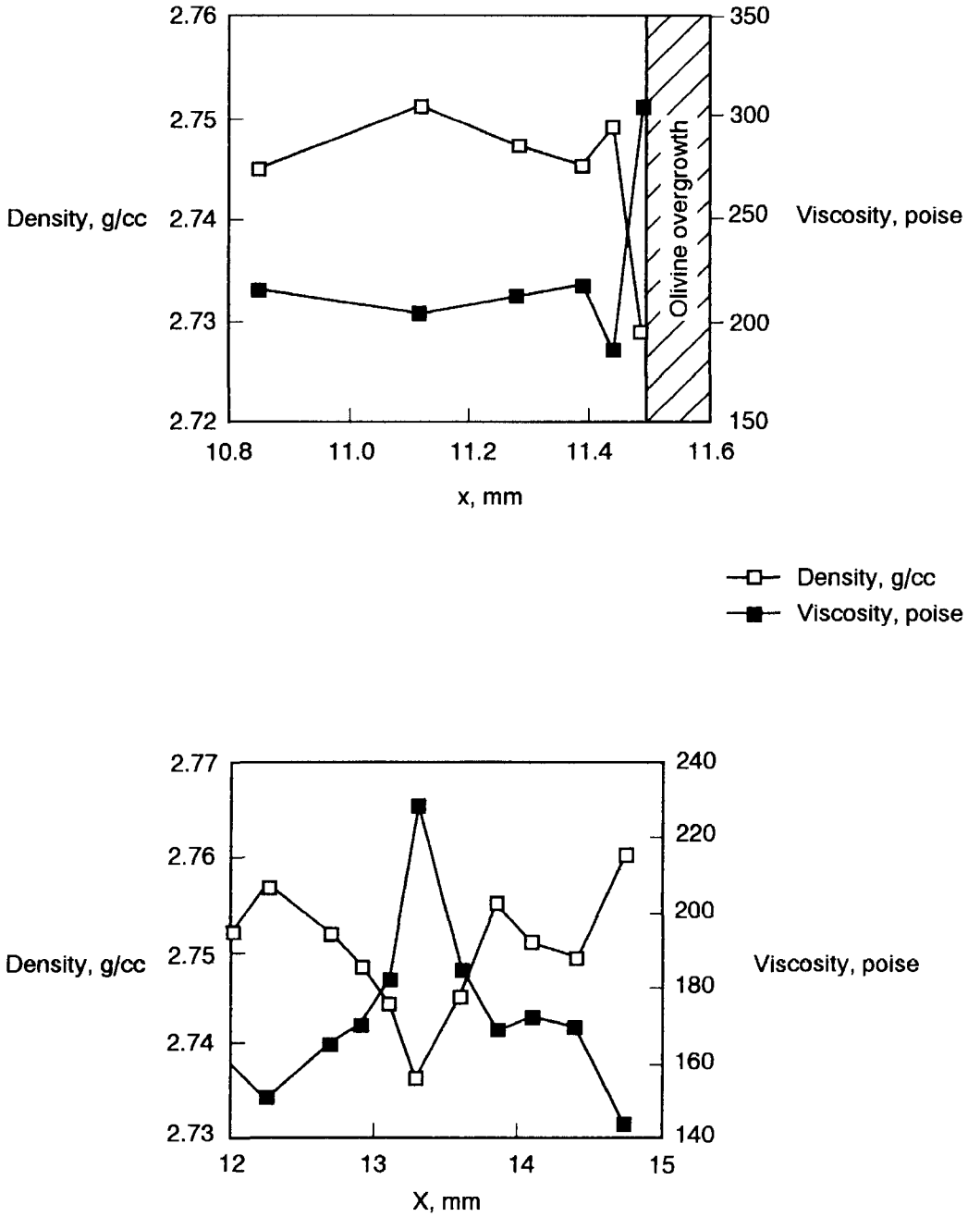

FIGS. 11 and 12. FIG. 11.(*top*) Density and viscosity profiles in the glass adjacent to the olivine overgrowth in experiment B. Calculations were made using the techniques of Bottinga and Weill (1970) and Shaw (1972) respectively. The partial molar volume for CoO was assumed to be identical to that of FeO for calculation purposes. Note the density decrease in the boundary layer of melt at the crystal-glass interface. FIG. 12. (*bottom*) Density and viscosity variations in glass above the olivine seed apex in experiment B. Data are from a horizontal line of points at 1 mm above the apex.

varying estimates of the diffusion coefficient. (As far as the current experiments are concerned, the figures are not relevant as seed crystals were shaped and mounted so as not to have faces horizontal such that there never was a condition in which boundary layer melt would have failed to convect.) For a horizontal boundary layer above an olivine seed or above a mush of growing olivines, a minimum thickness of (1080 μm at $D = 10^{-12}$ m^2s^{-1}) is required before it becomes buoyant, and this would require over 41 000 days to develop; the equivalent figures for $D = 10^{-9}$ m^2s^{-1} are 10790 μm and 4800 days. The slow rates compared with those seen in the experiments here indicate that the key factor in rates of convection is the orientation of the crystal sides. The net result is the addition of a slightly evolved melt (1–2 wt% depletion in MgO and FeO) to the bulk magma and their progressive mixing. Only if this evolved melt remained discrete could it build a compositionally contrasting top to a magma chamber.

Production of crystal overgrowth in these experiments required a reasonably high degree of supercooling ($-\Delta T$ of 20–40°C) and hence rapid crystal growth for compositional effects in the melt to be evident. In large bodies of magma much smaller supercoolings should be expected in rocks formed well beyond the chilled margins, and hence smaller growth rates and compositionally less pronounced boundary layers would result. In order to evaluate more realistically the effect of compositional convection on compositional evolution of magma, further experiments at smaller supercoolings need to be attempted to observe boundary layer production and convection. The conundrum, of course, is that such experiments will require much longer, possibly unrealistically long, run times for detectable compositional changes to develop in the glass of the run products.

Conclusions

The principal findings of the study are that:

(1) Maps prepared from X-ray count rate measurements at closely spaced analytical points are an ideal way to detect compositional variations in the glass that are too slight to be detectable optically.

(2) Olivine crystallization causes depletion of Co and Mg by up to 25% in a thin (up to 50 μm) boundary layer at the overgrowth-melt interface.

(3) The low density of this melt makes it buoyant in the surrounding melt.

(4) Boundary layer melt rises up the sides of the crystal seed and detaches from the upper corners of the crystal.

(5) Convection of boundary layer melt leads to vertical compositional differentiation of melt in experimental charges in long duration runs.

(6) Crystallization of Co-Mg spinel on the sidewalls of the crucibles is also responsible for producing melt with a lower density than the original melt. This process also contributes to the compositional differentiation of melt at the crucible walls in these experiments.

Acknowledgements

Jon Seedhouse is grateful to the NERC for a studentship to undertake this research. The work is supported by NERC research grant GR3/6509 to Colin Donaldson.

References

Bottinga, Y. and Weill, D.H. (1970) Densities of liquid silicate systems from partial molar volumes of oxide components. *Amer. J. Sci.*, **269**, 169–82.

Brearley, M. and Scarfe, C.M. (1986) Dissolution rates of upper mantle minerals in an alkali basalt melt at high pressure: an experimental study and implications for ultramafic xenolith survival. *J. Petrol.*, **27**, 1157–82.

Coons, W.E., Holloway, J.R. and Navrotsky, A.(1976) Co^{2+} as a chemical analogue for Fe^{2+} in high temperature experiments in basaltic systems. *Earth Planet. Sci. Lett.*, **30**, 303–8.

Coons, W.E. and Holloway, J.R. (1979) Cobaltous oxide as a chemical analogue for ferrous iron in experimental petrology: An alternative solution to the iron-loss problem. *Amer. Mineral.*, **64**, 1097–106.

Donaldson, C.H. (1975) Calculated diffusion coefficients and the growth rate of olivine in a basaltic magma. *Lithos*, **8**, 163–74.

Donaldson, C.H. (1976) An experimental investigation of olivine morphology. *Contrib. Mineral. Petrol.*, **57**, 187–213.

Donaldson, C.H. (1993) Convective fractionation during magnetite and hematite dissolution in silicate melts. *Mineral. Mag.*, **57**, 469–88.

Donaldson, C.H. and Hamilton, D.L. (1987) Compositional convection and layering in a rock melt. *Nature*, **327**, 413–5.

Hill, R.E.T. (1969) *The crystallization of basaltic melts as a function of oxygen fugacity.* Unpublished Ph.D. thesis. Queen's University, Belfast.

Hofmann, A.W. (1980) Diffusion in silicate melts: a critical review. In: *Physics of Magmatic Processes.* (R.B. Hargraves, ed.) Princeton University Press, 585 pp.

Kuo, L-C. and Kirkpatrick, R.J. (1985*a*) Kinetics of crystal dissolution in the system diopside-forsterite-silica. *Amer. J. Sci.*, **285**, 51–91.

Kuo, L-C. and Kirkpatrick, R.J. (1985*b*) Dissolution of mafic minerals and its implication for the ascent

velocities of peridotite-bearing basaltic magmas. *J. Geol.*, **93**, 691–700.

Martin, D., Griffiths, R.W. and Campbell, I.H. (1987) Compositional and thermal convection in magma chambers. *Contrib. Mineral. Petrol.*, **96**, 465–75.

Seedhouse, J.K. (1994) *Testing for compositional convection in silicate melts; crystal growth experiments and a petrographic study of a differentiated ring dyke*. PhD. Thesis, Univ. of St Andrews.

Shaw, H.R. (1972) Viscosities of magmatic silicate liquids: An empirical method of prediction. *Amer. J. Sci.*, **272**, 870–93.

Sparks, R.S.J., Huppert, H.E. and Turner, J.S. (1984) The fluid dynamics of evolving magma chambers. *Phil. Trans. Roy. Soc. London.*, **A310**, 511–34.

Tait, S.R., Huppert, H.E. and Sparks, R.S.J. (1984) The role of compositional convection in the formation of adcumulate rocks. *Lithos*, **17**, 139–46.

Tait, S.R. and Jaupart, C. (1992) Compositional convection in a reactive crystalline mush and melt differentiation. *J. Geoph. Res.*, **97**, 6735–56.

Turner, J.S. (1980) A fluid dynamical model of differentiation and layering in magma chambers. *Nature*, **285**, 213–5.

Turner, J.S. and Campbell, I.H. (1986) Convection and mixing in magma chambers. *Earth Sci. Rev.*, **23**, 255–352.

Wager, L.R., Brown, G.M. and Wadsworth, W.J. (1960) Types of igneous cumulates. *J. Petrol.*, **1**, 73–85.

Zhang, Y., Walker, D. and Lesher, C.E. (1989) Diffusive crystal dissolution. *Contrib. Mineral. Petrol.*, **102**, 492–513.

[*Revised manuscript received 10 July 1995*]